Observation of the isospin-violating decay J/ψ→φπ^{0}f_{0}(980)

M. Ablikim *et al.* (BESIII Collaboration)

Observation of the isospin-violating decay $J/\psi \to \phi\pi^0 f_0(980)$

M. Ablikim[1], M. N. Achasov[9,a], X. C. Ai[1], O. Albayrak[5], M. Albrecht[4], D. J. Ambrose[44], A. Amoroso[48A,48C], F. F. An[1], Q. An[45], J. Z. Bai[1], R. Baldini Ferroli[20A], Y. Ban[31], D. W. Bennett[19], J. V. Bennett[5], M. Bertani[20A], D. Bettoni[21A], J. M. Bian[43], F. Bianchi[48A,48C], E. Boger[23,h], O. Bondarenko[25], I. Boyko[23], R. A. Briere[5], H. Cai[50], X. Cai[1], O. Cakir[40A,b], A. Calcaterra[20A], G. F. Cao[1], S. A. Cetin[40B], J. F. Chang[1], G. Chelkov[23,c], G. Chen[1], H. S. Chen[1], H. Y. Chen[2], J. C. Chen[1], M. L. Chen[1], S. J. Chen[29], X. Chen[1], X. R. Chen[26], Y. B. Chen[1], H. P. Cheng[17], X. K. Chu[31], G. Cibinetto[21A], D. Cronin-Hennessy[43], H. L. Dai[1], J. P. Dai[34], A. Dbeyssi[14], D. Dedovich[23], Z. Y. Deng[1], A. Denig[22], I. Denysenko[23], M. Destefanis[48A,48C], F. De Mori[48A,48C], Y. Ding[27], C. Dong[30], J. Dong[1], L. Y. Dong[1], M. Y. Dong[1], S. X. Du[52], P. F. Duan[1], J. Z. Fan[39], J. Fang[1], S. S. Fang[1], X. Fang[45], Y. Fang[1], L. Fava[48B,48C], F. Feldbauer[22], G. Felici[20A], C. Q. Feng[45], E. Fioravanti[21A], M. Fritsch[14,22], C. D. Fu[1], Q. Gao[1], X. Y. Gao[2], Y. Gao[39], Z. Gao[45], I. Garzia[21A], C. Geng[45], K. Goetzen[10], W. X. Gong[1], W. Gradl[22], M. Greco[48A,48C], M. H. Gu[1], Y. T. Gu[12], Y. H. Guan[1], A. Q. Guo[1], L. B. Guo[28], Y. Guo[1], Y. P. Guo[22], Z. Haddadi[25], A. Hafner[22], S. Han[50], Y. L. Han[1], X. Q. Hao[15], F. A. Harris[42], K. L. He[1], Z. Y. He[30], T. Held[4], Y. K. Heng[1], Z. L. Hou[1], C. Hu[28], H. M. Hu[1], J. F. Hu[48A,48C], T. Hu[1], Y. Hu[1], G. M. Huang[6], G. S. Huang[45], H. P. Huang[50], J. S. Huang[15], X. T. Huang[33], Y. Huang[29], T. Hussain[47], Q. Ji[1], Q. P. Ji[30], X. B. Ji[1], X. L. Ji[1], L. L. Jiang[1], L. W. Jiang[50], X. S. Jiang[1], J. B. Jiao[33], Z. Jiao[17], D. P. Jin[1], S. Jin[1], T. Johansson[49], A. Julin[43], N. Kalantar-Nayestanaki[25], X. L. Kang[1], X. S. Kang[30], M. Kavatsyuk[25], B. C. Ke[5], R. Kliemt[14], B. Kloss[22], O. B. Kolcu[40B,d], B. Kopf[4], M. Kornicer[42], W. Kühn[24], A. Kupsc[49], W. Lai[1], J. S. Lange[24], M. Lara[19], P. Larin[14], C. Leng[48C], C. H. Li[1], Cheng Li[45], D. M. Li[52], F. Li[1], G. Li[1], H. B. Li[1], J. C. Li[1], Jin Li[32], K. Li[13], K. Li[33], Lei Li[3], P. R. Li[41], T. Li[33], W. D. Li[1], W. G. Li[1], X. L. Li[33], X. M. Li[12], X. N. Li[1], X. Q. Li[30], Z. B. Li[38], H. Liang[45], Y. F. Liang[36], Y. T. Liang[24], G. R. Liao[11], D. X. Lin[14], B. J. Liu[1], C. X. Liu[1], F. H. Liu[35], Fang Liu[1], Feng Liu[6], H. B. Liu[12], H. H. Liu[16], H. H. Liu[1], H. M. Liu[1], J. Liu[1], J. P. Liu[50], J. Y. Liu[1], K. Liu[39], K. Y. Liu[27], L. D. Liu[31], P. L. Liu[1], Q. Liu[41], S. B. Liu[45], X. Liu[26], X. X. Liu[41], Y. B. Liu[30], Z. A. Liu[1], Zhiqiang Liu[1], Zhiqing Liu[22], H. Loehner[25], X. C. Lou[1,e], H. J. Lu[17], J. G. Lu[1], R. Q. Lu[18], Y. Lu[1], Y. P. Lu[1], C. L. Luo[28], M. X. Luo[51], T. Luo[42], X. L. Luo[1], M. Lv[1], X. R. Lyu[41], F. C. Ma[27], H. L. Ma[1], L. L. Ma[33], Q. M. Ma[1], S. Ma[1], T. Ma[1], X. N. Ma[30], X. Y. Ma[1], F. E. Maas[14], M. Maggiora[48A,48C], Q. A. Malik[47], Y. J. Mao[31], Z. P. Mao[1], S. Marcello[48A,48C], J. G. Messchendorp[25], J. Min[1], T. J. Min[1], R. E. Mitchell[19], X. H. Mo[1], Y. J. Mo[6], C. Morales Morales[14], K. Moriya[19], N. Yu. Muchnoi[9,a], H. Muramatsu[43], Y. Nefedov[23], F. Nerling[14], I. B. Nikolaev[9,a], Z. Ning[1], S. Nisar[8], S. L. Niu[1], X. Y. Niu[1], S. L. Olsen[32], Q. Ouyang[1], S. Pacetti[20B], P. Patteri[20A], M. Pelizaeus[4], H. P. Peng[45], K. Peters[10], J. Pettersson[49], J. L. Ping[28], R. G. Ping[1], R. Poling[43], Y. N. Pu[18], M. Qi[29], S. Qian[1], C. F. Qiao[41], L. Q. Qin[33], N. Qin[50], X. S. Qin[1], Y. Qin[31], Z. H. Qin[1], J. F. Qiu[1], K. H. Rashid[47], C. F. Redmer[22], H. L. Ren[18], M. Ripka[22], G. Rong[1], Ch. Rosner[14], X. D. Ruan[12], V. Santoro[21A], A. Sarantsev[23,f], M. Savrié[21B], K. Schoenning[49], S. Schumann[22], W. Shan[31], M. Shao[45], C. P. Shen[2], P. X. Shen[30], X. Y. Shen[1], H. Y. Sheng[1], W. M. Song[1], X. Y. Song[1], S. Sosio[48A,48C], S. Spataro[48A,48C], G. X. Sun[1], J. F. Sun[15], S. S. Sun[1], Y. J. Sun[45], Y. Z. Sun[1], Z. J. Sun[1], Z. T. Sun[19], C. J. Tang[36], X. Tang[1], I. Tapan[40C], E. H. Thorndike[44], M. Tiemens[25], D. Toth[43], M. Ullrich[24], I. Uman[40B], G. S. Varner[42], B. Wang[30], B. L. Wang[41], D. Wang[31], D. Y. Wang[31], K. Wang[1], L. L. Wang[1], L. S. Wang[1], M. Wang[33], P. Wang[1], P. L. Wang[1], Q. J. Wang[1], S. G. Wang[31], W. Wang[1], X. F. Wang[39], Y. D. Wang[14], Y. F. Wang[1], Y. Q. Wang[22], Z. Wang[1], Z. G. Wang[1], Z. H. Wang[45], Z. Y. Wang[1], T. Weber[22], D. H. Wei[11], J. B. Wei[31], P. Weidenkaff[22], S. P. Wen[1], U. Wiedner[4], M. Wolke[49], L. H. Wu[1], Z. Wu[1], L. G. Xia[39], Y. Xia[18], D. Xiao[1], Z. J. Xiao[28], Y. G. Xie[1], Q. L. Xiu[1], G. F. Xu[1], L. Xu[1], Q. J. Xu[13], Q. N. Xu[41], X. P. Xu[37], L. Yan[45], W. B. Yan[45], W. C. Yan[45], Y. H. Yan[18], H. X. Yang[1], L. Yang[50], Y. Yang[6], Y. X. Yang[11], H. Ye[1], M. Ye[1], M. H. Ye[7], J. H. Yin[1], B. X. Yu[1], C. X. Yu[30], H. W. Yu[31], J. S. Yu[26], C. Z. Yuan[1], W. L. Yuan[29], Y. Yuan[1], A. Yuncu[40B,g], A. A. Zafar[47], A. Zallo[20A], Y. Zeng[18], B. X. Zhang[1], B. Y. Zhang[1], C. Zhang[29], C. C. Zhang[1], D. H. Zhang[1], H. H. Zhang[38], H. Y. Zhang[1], J. J. Zhang[1], J. L. Zhang[1], J. Q. Zhang[1], J. W. Zhang[1], J. Y. Zhang[1], J. Z. Zhang[1], K. Zhang[1], L. Zhang[1], S. H. Zhang[1], X. Y. Zhang[33], Y. Zhang[1], Y. H. Zhang[1], Y. T. Zhang[45], Z. H. Zhang[6], Z. P. Zhang[45], Z. Y. Zhang[50], G. Zhao[1], J. W. Zhao[1], J. Y. Zhao[1], J. Z. Zhao[1], Lei Zhao[45], Ling Zhao[1], M. G. Zhao[30], Q. Zhao[1], Q. W. Zhao[1], S. J. Zhao[52], T. C. Zhao[1], Y. B. Zhao[1], Z. G. Zhao[45], A. Zhemchugov[23,h], B. Zheng[46], J. P. Zheng[1], W. J. Zheng[33], Y. H. Zheng[41], B. Zhong[28], L. Zhou[1], Li Zhou[30], X. Zhou[50], X. K. Zhou[45], X. R. Zhou[45], X. Y. Zhou[1], K. Zhu[1], K. J. Zhu[1], S. Zhu[1], X. L. Zhu[39], Y. C. Zhu[45], Y. S. Zhu[1], Z. A. Zhu[1], J. Zhuang[1], L. Zotti[48A,48C], B. S. Zou[1], J. H. Zou[1]

(BESIII Collaboration)

[1] *Institute of High Energy Physics, Beijing 100049, People's Republic of China*
[2] *Beihang University, Beijing 100191, People's Republic of China*
[3] *Beijing Institute of Petrochemical Technology, Beijing 102617, People's Republic of China*
[4] *Bochum Ruhr-University, D-44780 Bochum, Germany*
[5] *Carnegie Mellon University, Pittsburgh, Pennsylvania 15213, USA*
[6] *Central China Normal University, Wuhan 430079, People's Republic of China*
[7] *China Center of Advanced Science and Technology, Beijing 100190, People's Republic of China*
[8] *COMSATS Institute of Information Technology, Lahore, Defence Road, Off Raiwind Road, 54000 Lahore, Pakistan*
[9] *G.I. Budker Institute of Nuclear Physics SB RAS (BINP), Novosibirsk 630090, Russia*
[10] *GSI Helmholtzcentre for Heavy Ion Research GmbH, D-64291 Darmstadt, Germany*
[11] *Guangxi Normal University, Guilin 541004, People's Republic of China*
[12] *GuangXi University, Nanning 530004, People's Republic of China*
[13] *Hangzhou Normal University, Hangzhou 310036, People's Republic of China*

[14] Helmholtz Institute Mainz, Johann-Joachim-Becher-Weg 45, D-55099 Mainz, Germany

[15] Henan Normal University, Xinxiang 453007, People's Republic of China

[16] Henan University of Science and Technology, Luoyang 471003, People's Republic of China

[17] Huangshan College, Huangshan 245000, People's Republic of China

[18] Hunan University, Changsha 410082, People's Republic of China

[19] Indiana University, Bloomington, Indiana 47405, USA

[20] (A)INFN Laboratori Nazionali di Frascati, I-00044, Frascati, Italy; (B)INFN and University of Perugia, I-06100, Perugia, Italy

[21] (A)INFN Sezione di Ferrara, I-44122, Ferrara, Italy; (B)University of Ferrara, I-44122, Ferrara, Italy

[22] Johannes Gutenberg University of Mainz, Johann-Joachim-Becher-Weg 45, D-55099 Mainz, Germany

[23] Joint Institute for Nuclear Research, 141980 Dubna, Moscow region, Russia

[24] Justus Liebig University Giessen, II. Physikalisches Institut, Heinrich-Buff-Ring 16, D-35392 Giessen, Germany

[25] KVI-CART, University of Groningen, NL-9747 AA Groningen, The Netherlands

[26] Lanzhou University, Lanzhou 730000, People's Republic of China

[27] Liaoning University, Shenyang 110036, People's Republic of China

[28] Nanjing Normal University, Nanjing 210023, People's Republic of China

[29] Nanjing University, Nanjing 210093, People's Republic of China

[30] Nankai University, Tianjin 300071, People's Republic of China

[31] Peking University, Beijing 100871, People's Republic of China

[32] Seoul National University, Seoul, 151-747 Korea

[33] Shandong University, Jinan 250100, People's Republic of China

[34] Shanghai Jiao Tong University, Shanghai 200240, People's Republic of China

[35] Shanxi University, Taiyuan 030006, People's Republic of China

[36] Sichuan University, Chengdu 610064, People's Republic of China

[37] Soochow University, Suzhou 215006, People's Republic of China

[38] Sun Yat-Sen University, Guangzhou 510275, People's Republic of China

[39] Tsinghua University, Beijing 100084, People's Republic of China

[40] (A)Istanbul Aydin University, 34295 Sefakoy, Istanbul, Turkey; (B)Dogus University, 34722 Istanbul, Turkey; (C)Uludag University, 16059 Bursa, Turkey

[41] University of Chinese Academy of Sciences, Beijing 100049, People's Republic of China

[42] University of Hawaii, Honolulu, Hawaii 96822, USA

[43] University of Minnesota, Minneapolis, Minnesota 55455, USA

[44] University of Rochester, Rochester, New York 14627, USA

[45] University of Science and Technology of China, Hefei 230026, People's Republic of China

[46] University of South China, Hengyang 421001, People's Republic of China

[47] University of the Punjab, Lahore-54590, Pakistan

[48] (A)University of Turin, I-10125, Turin, Italy; (B)University of Eastern Piedmont, I-15121, Alessandria, Italy; (C)INFN, I-10125, Turin, Italy

[49] Uppsala University, Box 516, SE-75120 Uppsala, Sweden

[50] Wuhan University, Wuhan 430072, People's Republic of China

[51] Zhejiang University, Hangzhou 310027, People's Republic of China

[52] Zhengzhou University, Zhengzhou 450001, People's Republic of China

[a] Also at the Novosibirsk State University, Novosibirsk, 630090, Russia

[b] Also at Ankara University, 06100 Tandogan, Ankara, Turkey

[c] Also at the Moscow Institute of Physics and Technology, Moscow 141700, Russia and at the Functional Electronics Laboratory, Tomsk State University, Tomsk, 634050, Russia

[d] Currently at Istanbul Arel University, 34295 Istanbul, Turkey

[e] Also at University of Texas at Dallas, Richardson, Texas 75083, USA

[f] Also at the NRC "Kurchatov Institute", PNPI, 188300, Gatchina, Russia

[g] Also at Bogazici University, 34342 Istanbul, Turkey

[h] Also at the Moscow Institute of Physics and Technology, Moscow 141700, Russia

1

1

Using a sample of 1.31 billion J/ψ events collected with the BESIII detector at the BEPCII collider, the decays $J/\psi \to \phi\pi^+\pi^-\pi^0$ and $J/\psi \to \phi\pi^0\pi^0\pi^0$ are investigated. The isospin violating decay $J/\psi \to \phi\pi^0 f_0(980)$ with $f_0(980) \to \pi\pi$, is observed for the first time. The width of the $f_0(980)$ obtained from the dipion mass spectrum is found to be much smaller than the world average value. In the $\pi^0 f_0(980)$ mass spectrum, there is evidence of $f_1(1285)$ production. By studying the decay $J/\psi \to \phi\eta'$, the branching fractions of $\eta' \to \pi^+\pi^-\pi^0$ and $\eta' \to \pi^0\pi^0\pi^0$, as well as their ratio, are

also measured.

I. INTRODUCTION

The nature of the scalar meson $f_0(980)$ is a long-standing puzzle. It has been interpreted as a $q\bar{q}$ state, a $K\bar{K}$ molecule, a glueball, and a four-quark state (see the review in Ref. [1]). Further insights are expected from studies of $f_0(980)$ mixing with the $a_0^0(980)$ [2], evidence for which was found in a recent BESIII analysis of J/ψ and χ_{c1} decays [3]. BESIII also observed a large isospin violation in J/ψ radiatively decaying into $\pi^+\pi^-\pi^0$ and $\pi^0\pi^0\pi^0$ involving the intermediate decay $\eta(1405) \to \pi^0 f_0(980)$ [4]. In this study, the $f_0(980)$ width was found to be 9.5 ± 1.1 MeV/c^2. One proposed explanation for this anomalously narrow width and the observed large isospin violation, which cannot be caused by $a_0^0(980) - f_0(980)$ mixing, is the triangle singularity mechanism [5, 6].

The decays $J/\psi \to \phi\pi^+\pi^-\pi^0$ and $J/\psi \to \phi\pi^0\pi^0\pi^0$ are similar to the radiative decays $J/\psi \to \gamma\pi^+\pi^-\pi^0/\pi^0\pi^0\pi^0$ as the ϕ and γ share the same spin and parity quantum numbers. Any intermediate $f_0(980)$ would be noticeable in the $\pi\pi$ mass spectra. At the same time, a study of the decay $J/\psi \to \phi\eta'$ would enable a measurement of the branching fractions for $\eta' \to \pi^+\pi^-\pi^0$ and $\eta' \to \pi^0\pi^0\pi^0$. The recently measured $\mathcal{B}(\eta' \to 3\pi^0) = (3.56 \pm 0.40) \times 10^{-3}$ [4] from a study of the decay $J/\psi \to \gamma\eta'$ was found to be nearly 4σ higher than the previous value $(1.73 \pm 0.23) \times 10^{-3}$ from studies of the reaction $\pi^- p \to n(6\gamma)$ [7–9][1]. Additionally, the isospin-violating decays $\eta' \to \pi^+\pi^-\pi^0/\pi^0\pi^0\pi^0$ provide a means to extract the d, u quark mass difference $m_d - m_u$ [10].

This paper reports a study of $J/\psi \to \phi\pi^+\pi^-\pi^0$ and $J/\psi \to \phi\pi^0\pi^0\pi^0$ with $\phi \to K^+K^-$ based on a sample of $(1.311 \pm 0.011) \times 10^9$ [11, 12] J/ψ events accumulated with the BESIII detector in 2009 and 2012.

II. DETECTOR AND MONTE CARLO SIMULATION

The BESIII detector [13] is a magnetic spectrometer located at the Beijing Electron-Positron Collider (BEPCII), which is a double-ring e^+e^- collider with a design luminosity of 10^{33} cm^{-2}s^{-1} at a center of mass (c.m.) energy of 3.773 GeV. The cylindrical core of the BESIII detector consists of a helium-based main drift chamber (MDC), a plastic scintillator time-of-flight system (TOF), and a CsI(Tl) electromagnetic calorimeter

---

[1] The PDG [1] gives an average value, $\Gamma(\eta' \to 3\pi^0)/\Gamma(\eta' \to \pi^0\pi^0\eta) = 0.0078 \pm 0.0010$, of three measurements [7–9]. $\mathcal{B}(\eta' \to 3\pi^0)$ is calculated using $\mathcal{B}(\eta' \to \pi^0\pi^0\eta) = 0.222 \pm 0.008$ [1], assuming the uncertainties are independent.

(EMC). All are enclosed in a superconducting solenoidal magnet providing a 1.0 T (0.9 T in 2012) magnetic field. The solenoid is supported by an octagonal flux-return yoke with resistive plate counter muon identifier modules interleaved with steel. The acceptance for charged tracks and photons is 93% of 4π solid angle. The charged-particle momentum resolution is 0.5% at 1 GeV/c, and the specific energy loss (dE/dx) resolution is better than 6%. The photon energy is measured in the EMC with a resolution of 2.5% (5%) at 1 GeV in the barrel (endcaps). The time resolution of the TOF is 80 ps (110 ps) in the barrel (endcaps). The BESIII offline software system framework, based on the GAUDI package [14], provides standard interfaces and utilities for event simulation, data processing and physics analysis.

Monte Carlo (MC) simulation, based on the GEANT4 [15] package, is used to simulate the detector response, study the background and determine efficiencies. For this analysis, we use a phase space MC sample to describe the three body decay $J/\psi \to \phi\pi^0 f_0(980)$, while the angular distributions are considered in the decays $J/\psi \to \phi f_1(1285) \to \phi\pi^0 f_0(980)$ and $J/\psi \to \phi\eta'$. In the MC samples, the width of the $f_0(980)$ is fixed to be 15.3 MeV/c^2, which is obtained from a fit to data as described below. An inclusive MC sample of 1.2 billion J/ψ decays is used to study the background. For this MC sample, the generator BESEVTGEN [16, 17] is used to generate the known J/ψ decays according to their measured branching fractions [1] while LUNDCHARM [18] is used to generate the remaining unknown decays.

III. EVENT SELECTION

Charged tracks are reconstructed from hits in the MDC and selected by requiring that $|\cos\theta| < 0.93$, where θ is the polar angle measured in the MDC, and that the point of closest approach to the e^+e^- interaction point is within ± 10 cm in the beam direction and within 1 cm in the plane perpendicular to the beam direction. TOF and dE/dx information are combined to calculate the particle identification (PID) probabilities for the pion, kaon and proton hypotheses. For each photon, the energy deposited in the EMC must be at least 25 MeV (50 MeV) in the region of $|\cos\theta| < 0.8$ ($0.86 < |\cos\theta| < 0.92$). To exclude showers that originate from charged tracks, the angle between a photon candidate and the closest charged track must be larger than $10°$. The timing information from the EMC is used to suppress electronics noise and unrelated energy deposits.

To be accepted as a $J/\psi \to K^+K^-\pi^+\pi^-\pi^0$ decay, a candidate event is required to have four charged tracks with zero net charge and at least two photons. The two oppositely charged tracks with an invariant mass closest

to the nominal mass of the ϕ are assigned as being kaons, while the remaining tracks are assigned as being pions. To avoid misidentification, kaon tracks are required to have a PID probability of being a kaon that is larger than that of being a pion. A 5-constraint kinematic fit is applied to the candidate events under the hypothesis $J/\psi \to K^+K^-\pi^+\pi^-\gamma\gamma$. This includes a constraint that the total four-momenta of the selected particles must be equal to the initial four-momentum of the colliding beams (4-constraint) and that the invariant mass of the two photons must be the nominal mass of the π^0 (1-constraint). If more than 2 photon candidates are found in the event, the combination with the minimum $\chi^2(5C)$ from the kinematic fit is retained. Only events with a $\chi^2(5C)$ less than 100 are accepted. Events with a $K^\pm\pi^\mp$ invariant mass satisfying $|M(K^\pm\pi^\mp) - M(K^{*0})| < 0.050$ GeV/c^2 are rejected in order to suppress the background containing K^{*0} or $\bar{K}^{*0}$ intermediate states.

To be accepted as a $J/\psi \to K^+K^-\pi^0\pi^0\pi^0$ decay, a candidate event is required to have two oppositely charged tracks and at least six photons. For both tracks, the PID probability of being a kaon must be larger than that of being a pion. The six photons are selected and paired by minimizing the quantity $\frac{(M(\gamma_1\gamma_2)-M_{\pi^0})^2}{\sigma_{\pi^0}^2} + \frac{(M(\gamma_3\gamma_4)-M_{\pi^0})^2}{\sigma_{\pi^0}^2} + \frac{(M(\gamma_5\gamma_6)-M_{\pi^0})^2}{\sigma_{\pi^0}^2}$, where $M(\gamma_i\gamma_j)$ is the mass of $\gamma_i\gamma_j$, and M_{π^0} and σ_{π^0} are the nominal mass and reconstruction resolution of the π^0 respectively. A 7-constraint kinematic fit is performed to the $J/\psi \to K^+K^-6\gamma$ hypothesis, where the constraints include the four-momentum constraint to the four-momentum of the colliding beams and three constraints of photon pairs to have invariant masses equal to the π^0. Events with a $\chi^2(7C)$ less than 90 are accepted.

Figures 1 (a) and (b) show $M(3\pi)$ versus $M(K^+K^-)$ for the two final states respectively. Clear signals from $\phi\eta$ and $\phi\eta'$ with $\eta' \to 3\pi^0$ are noticeable. In Fig. 1 (a), horizontal bands are noticeable from ω and ϕ decaying into $\pi^+\pi^-\pi^0$ in the background channel $J/\psi \to \omega/\phi K^+K^-$.

To search for the decay $J/\psi \to \phi\pi^0 f_0(980)$, we focus on the region $0.99 < M(K^+K^-) < 1.06$ GeV/c^2 and $0.850 < M(\pi\pi) < 1.150$ GeV/c^2. The $M(K^+K^-)$ spectra are shown in Fig. 2. Clear ϕ signals are visible. The $M(\pi^+\pi^-)$ and $M(\pi^0\pi^0)$ spectra for the ϕ signal region, which is defined by requiring $1.015 < M(K^+K^-) < 1.025$ GeV/c^2, are presented in Fig. 3 (a) and (b) respectively. A clear $f_0(980)$ peak exists for the $\pi^+\pi^-$ mode. The $M(f_0(980)[\pi\pi]\pi^0)$ spectra for the $f_0(980)$ signal region, defined as $0.960 < M(\pi\pi) < 1.020$ GeV/c^2, are presented in Fig. 4. There is evidence of a resonance around 1.28 GeV/c^2 for the decay $f_0(980) \to \pi^+\pi^-$, which will be identified as the $f_1(1285)$ [2].

To ensure that the observed f_0 and f_1 signals do not originate from background processes, the same selection

---

[2] For simplicity, $f_0(980)$ and $f_1(1285)$ will be written as f_0 and f_1 respectively throughout this paper.
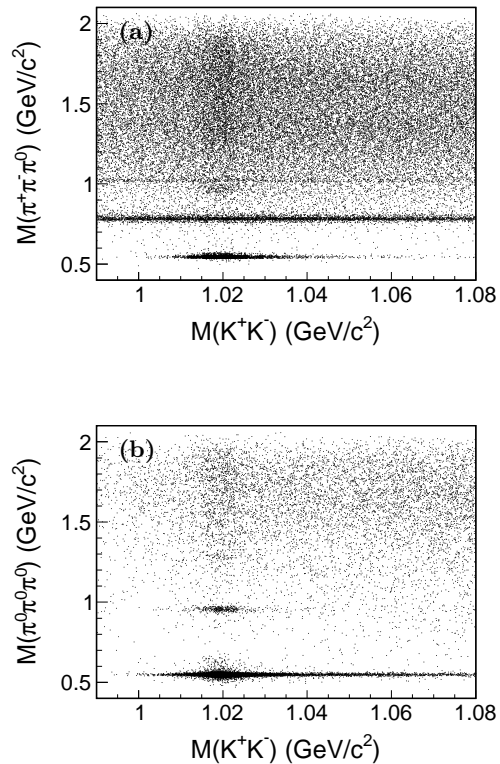

FIG. 1. Scatter plots of (a) $M(\pi^+\pi^-\pi^0)$ versus $M(K^+K^-)$ and (b) $M(\pi^0\pi^0\pi^0)$ versus $M(K^+K^-)$.

criteria as described above are applied to an MC sample of 1.2 billion inclusive J/ψ decays which does not contain the signal decay. As expected, neither an f_1 nor an f_0 is observed from the inclusive MC sample. The non-ϕ background is studied using data from the ϕ sideband regions ($0.990 < M(K^+K^-) < 1.000$ GeV/c^2 and $1.040 < M(K^+K^-) < 1.050$ GeV/c^2), which are given by the hatched histograms in Fig. 3 and Fig. 4 and in which no f_0 or f_1 signals are observed.

IV. SIGNAL EXTRACTION OF $J/\psi \to \phi\pi^0 f_0(980)$

Figures 3 (a) and (b) show the $\pi^+\pi^-$ and $\pi^0\pi^0$ mass spectra for events with $M(K^+K^-)$ in the ϕ signal region (the black dots) and sideband regions (the hatched histogram scaled by a normalization factor, C). Events in the ϕ sideband regions are normalized in the following way. A fit is performed to the K^+K^- mass spectrum, where the ϕ signal is described by a Breit-Wigner function convoluted with a Gaussian resolution function and the background is described by a second-order polynomial. The mass and width of the ϕ resonance are fixed to their world average values [1] and the mass resolution is allowed to float. The normalization factor C is defined as $A_{\rm sig}/A_{\rm sbd}$, where $A_{\rm sig}$ ($A_{\rm sbd}$) is the area of the background function from the fits in the signal (sideband)

region. The results of the fits are shown in Fig. 2 (a) and (b).

To extract the signal yield of $J/\psi \to \phi\pi^0 f_0$, a simultaneous unbinned maximum likelihood fit is performed to the $\pi^+\pi^-$ and $\pi^0\pi^0$ mass spectra. The lineshape of the f_0 signal is different from that of the Flatté-form resonance observed in the decays $J/\psi \to \phi\pi^+\pi^-$ and $J/\psi \to \phi K^+K^-$ [19]. A Breit-Wigner function convoluted with a Gaussian mass resolution function is used to describe the f_0 signal. The mass resolutions of the f_0 in the $M(\pi^+\pi^-)$ and $M(\pi^0\pi^0)$ spectra are determined from MC simulations. The non-ϕ background is parameterized with a straight line, which is determined from a fit to the data in the ϕ sideband regions. The size of this polynomial is fixed according to the normalized number of background events under the ϕ peak, $N_{\text{bkg}} = CN_{\text{sbd}}$, where N_{sbd} is the number of events falling in the ϕ sideband regions and C is the normalization factor obtained above. Another straight line is used to account for the remaining background from $J/\psi \to \phi\pi^0\pi\pi$ without f_0 decaying into $\pi\pi$.

The mass and width of the f_0 are constrained to be the same for both the $K^+K^-\pi^+\pi^-\pi^0$ and the $K^+K^-\pi^0\pi^0\pi^0$ final states. The fit yields the values $M(f_0) = 989.4 \pm 1.3$ MeV/c^2 and $\Gamma(f_0) = 15.3 \pm 4.7$ MeV/c^2, with the number of events $N = 354.7 \pm 63.3$ for the $\pi^+\pi^-$ mode and 69.8 ± 21.1 for the $\pi^0\pi^0$ mode. The statistical significance is determined by the changes of the log likelihood value and the number of degrees of freedom in the fit with and without the signal [20]. The significance of the f_0 signal is 9.4σ in the $K^+K^-\pi^+\pi^-\pi^0$ final state and 3.2σ in the $K^+K^-\pi^0\pi^0\pi^0$ final state. The measured mass and width obtained from the invariant dipion mass spectrum are consistent with those from the study of the decay $J/\psi \to \gamma\eta(1405) \to \gamma\pi^0 f_0(980)$ [4]. It is worth noting that the measured width of the f_0 observed in the dipion mass spectrum is much smaller than the world average value of 40-100 MeV [1].

V. SIGNAL EXTRACTION OF $J/\psi \to \phi f_1(1285)$ WITH $f_1(1285) \to \pi^0 f_0(980)$

Figures 4 (a) and (b) show the $\pi^+\pi^-\pi^0$ and $\pi^0\pi^0\pi^0$ mass spectra in the ϕ and f_0 signal region (the black dots) and sideband regions (the hatched histogram). The f_0 sideband regions are defined as $0.850 < M(\pi\pi) < 0.910$ GeV/c^2 and $1.070 < M(\pi\pi) < 1.130$ GeV/c^2. In Fig. 4, events in the 2-dimensional sideband regions are weighted as follows. Events that fall in only the ϕ or $f_0(980)$ sideband regions are given a weight 0.5 to take into account the non-ϕ or non-$f_0(980)$ background while those that fall in both the ϕ and the $f_0(980)$ sideband regions are given a weight -0.25 to compensate for the double counting of the non-ϕ and non-$f_0(980)$ background. There is evidence of a resonance around 1.28 GeV/c^2 that is not noticeable in the 2-dimensional sideband regions. By studying an MC sample of the de-
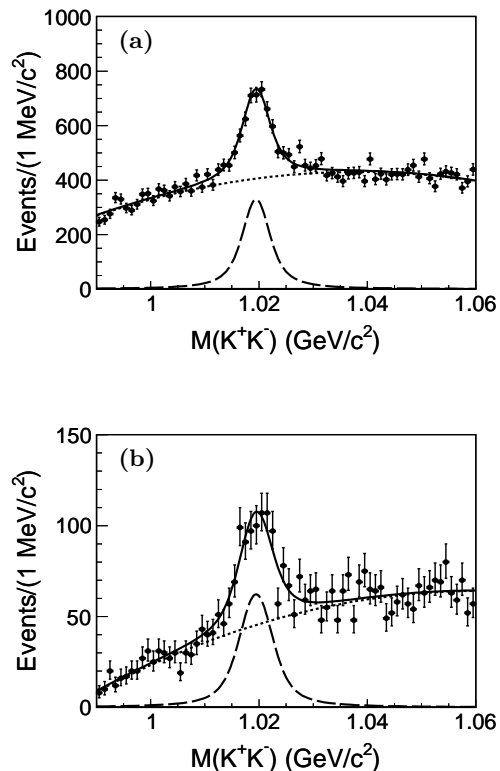

FIG. 2. Fits to the $M(K^+K^-)$ mass spectra for the mode (a) $f_0(980) \to \pi^+\pi^-$ and (b) $f_0(980) \to \pi^0\pi^0$. The solid curve is the full fit; the long-dashed curve is the ϕ signal while the short-dashed curve is the background.

cay $J/\psi \to \phi f_1 \to$ anything, we find that the decay $f_1 \to \pi^0\pi^0\eta/\pi^0 a_0^0$ [3] with $\eta \to \gamma\gamma$ contributes as a peaking background for the decay $f_1 \to \pi^0\pi^0\pi^0$. The yield of this peaking background is calculated to be 3.1 ± 0.6 using the relevant branching fractions [4] [1] and the efficiency determined from an MC simulation. A simultaneous unbinned maximum likelihood fit is performed to the $M(\pi^+\pi^-\pi^0)$ and $M(\pi^0\pi^0\pi^0)$ distributions. The f_1 signal is described by a Breit-Wigner function convoluted with a Gaussian mass resolution function. The shape of the peaking background $f_1 \to \pi^0\pi^0\eta/\pi^0 a_0^0$ is determined from an exclusive MC sample and its size is fixed to be 3.1. A second order polynomial function is used to describe the remaining background. The mass resolutions of the f_1 in $M(\pi^+\pi^-\pi^0)$ and $M(\pi^0\pi^0\pi^0)$ are determined from MC simulations.

The fit to $M(\pi^+\pi^-\pi^0)$ and $M(\pi^0\pi^0\pi^0)$ distributions yields the values $M(f_1) = 1287.4 \pm 3.0$ MeV/c^2 and $\Gamma(f_1) = 18.3 \pm 6.3$ MeV/c^2, with the number of events

---

[3] For simplicity, $a_0(980)$ and $a_0^0(980)$ are written as a_0 and a_0^0 respectively throughout this paper.

[4] We assume that $\mathcal{B}(f_1 \to \pi^0\pi^0\eta) = \frac{1}{3}\mathcal{B}(f_1 \to \pi\pi\eta)$, $\mathcal{B}(f_1 \to \pi^0 a_0^0) = \frac{1}{3}\mathcal{B}(f_1 \to \pi a_0)$, and $\mathcal{B}(a_0^0 \to \pi^0\eta) = 100\%$.
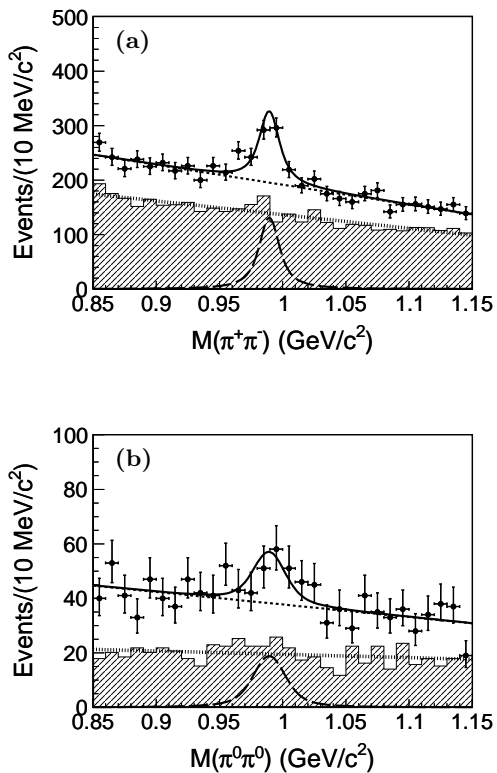
FIG. 3. The spectra (a) $M(\pi^+\pi^-)$ and (b) $M(\pi^0\pi^0)$ (three entries per event) with K^+K^- in the ϕ signal region (the black dots) and in the ϕ sideband regions (the hatched histogram). The solid curve is the full fit; the long-dashed curve is the $f_0(980)$ signal; the dotted line is the non-ϕ background and the short-dashed line is the total background.

FIG. 4. The spectra of (a) $M(\pi^+\pi^-\pi^0)$ and (b) $M(\pi^0\pi^0\pi^0)$ in the ϕ and $f_0(980)$ signal region (the black dots with error bars) and in the sideband regions (the hatched histogram). The solid curve is the result of the fit, the long-dashed curve is the $f_1(1285)$ signal, and the short-dashed curve is the background. In (b), the dotted curve represents the peaking background from the decay $f_1(1285) \to \pi^0\pi^0\eta/\pi^0 a_0^0$ with $\eta \to \gamma\gamma$.

$N = 78.2 \pm 19.3$ for the $K^+K^-\pi^+\pi^-\pi^0$ final state and $N = 8.7 \pm 6.8$ (< 18.2 at the 90% Confidence Level (C. L.)) for the $K^+K^-\pi^0\pi^0\pi^0$ final state. The mass and width are consistent with those of the axial-vector meson f_1 [1] [5]. The statistical significance of the f_1 signal is 5.2σ for the $K^+K^-\pi^+\pi^-\pi^0$ final state and 1.8σ for the $K^+K^-\pi^0\pi^0\pi^0$ final state. From the fit results, summarized in Table I, it is clear that the production of a single f_1 resonance cannot account for all of the $f_0\pi^0$ events above the background.

VI. SIGNAL EXTRACTION OF $J/\psi \to \phi\eta'$

For the decay $J/\psi \to \phi\eta' \to K^+K^-\pi^+\pi^-\pi^0$, the decays $J/\psi \to \phi\eta' \to K^+K^-\gamma\rho[(\gamma)\pi^+\pi^-]$ and $J/\psi \to \phi\eta' \to K^+K^-\gamma\omega[\pi^+\pi^-\pi^0]$ produce peaking background.

---

[5] Here we assume that the contribution of the pseudoscalar $\eta(1295)$ is small as no significant $\eta(1295)$ signals were found in the $\pi^+\pi^-\eta$ mass spectrum from a study of $J/\psi \to \phi\pi^+\pi^-\eta$ [21].
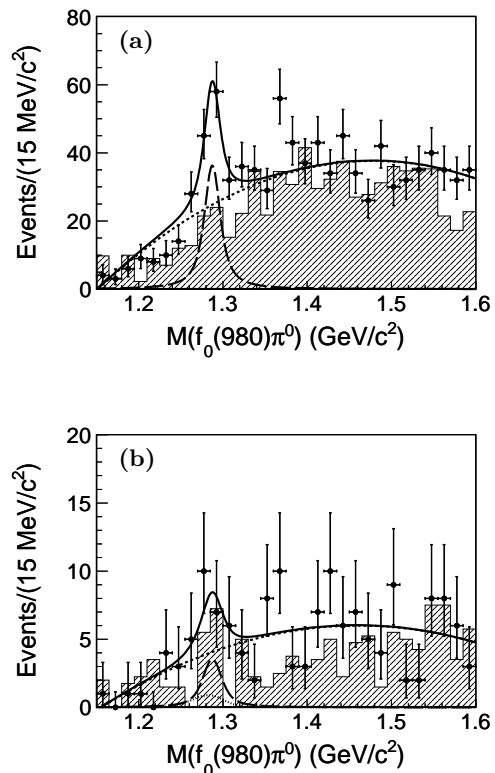
To reduce the former peaking background which is dominant, events with $0.920 < M(\gamma\pi^+\pi^-) < 0.970$ GeV/c^2 are rejected.

As the amount of background for the decay $J/\psi \to \phi\eta' \to K^+K^-\pi^0\pi^0\pi^0$ is relatively small, the ϕ signal and sideband regions are expanded to be $1.010 < M(K^+K^-) < 1.030$ GeV/c^2 and $1.040 < M(K^+K^-) < 1.060$ GeV/c^2, respectively. A peaking background for this decay comes from the decay $J/\psi \to \phi\eta' \to K^+K^-\pi^0\pi^0\eta[\gamma\gamma]$. To reduce this background, events with any photon pair mass in the range $0.510 < M(\gamma\gamma) < 0.580$ GeV/c^2 are rejected.

Figures 5 (a) and (b) show the final $\pi^+\pi^-\pi^0$ and $\pi^0\pi^0\pi^0$ mass spectra for the ϕ signal (the black dots) and sideband (the hatched histogram) regions. By analyzing data in the ϕ sideband regions and the inclusive MC sample, we find that the contribution from the decay $J/\psi \to K^+K^-\eta'$ is negligible.

An unbinned likelihood fit is performed to obtain the signal yields. The η' signal shape is determined by sampling a histogram from an MC simulation convoluted with a Gaussian function to compensate for the reso-
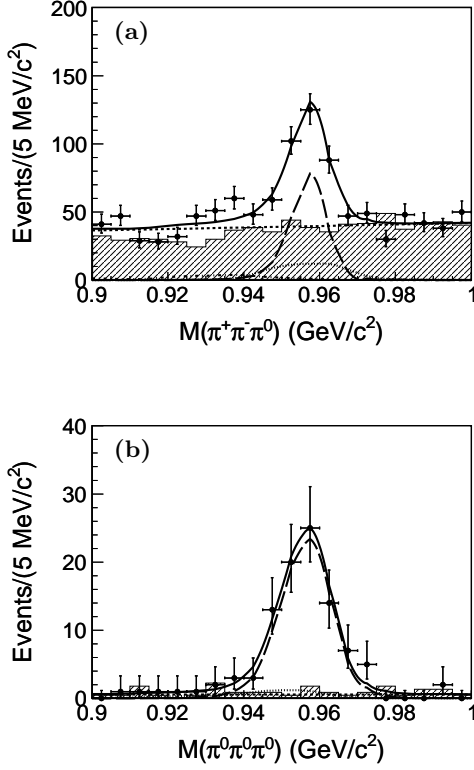
FIG. 5. The spectra (a) $M(\pi^+\pi^-\pi^0)$ and (b) $M(\pi^0\pi^0\pi^0)$ with K^+K^- in the ϕ signal region (the black dots) and side-band regions (the hatched histogram). The solid curve is the result of the fit, the long-dashed curve is the η' signal, and the short-dashed line is the polynomial background. In (a), the dotted and dot-dashed curves represent the peaking background $\eta' \to \gamma\rho \to \gamma(\gamma)\pi^+\pi^-$ and $\eta' \to \gamma\omega \to \gamma\pi^+\pi^-\pi^0$, respectively. In (b), the dotted curve represents the peaking background $\eta' \to \pi^0\pi^0\eta$ with $\eta \to \gamma\gamma$.

lution difference between the data and the MC sample. The shape of the peaking background is determined from exclusive MC samples, where the relative size of the background shape is determined using the relevant branching fractions in the PDG [1]. The non-peaking background is described by a first-order (zeroth-order) polynomial for the $\eta' \to \pi^+\pi^-\pi^0$ ($\pi^0\pi^0\pi^0$) decay. The number of events are determined to be $N = 183.3 \pm 21.0$ for the $K^+K^-\pi^+\pi^-\pi^0$ final state and 77.6 ± 9.6 for the $K^+K^-\pi^0\pi^0\pi^0$ final state.

VII. BRANCHING FRACTIONS MEASUREMENT

Table I summarizes the signal yields extracted from the fits for each decay. Equations (1) and (2) give the formulae used to calculate the branching fractions, where n is the number of π^0s in the final state X. N^{obs} and ϵ are the signal yield from the fits and efficiency from

TABLE I. Summary of the observed number of events (N^{obs}, the errors are statistical only.).

Decay mode	N^{obs}
$J/\psi \to \phi\pi^0 f_0$, $f_0 \to \pi^+\pi^-$	354.7 ± 63.3
$J/\psi \to \phi\pi^0 f_0$, $f_0 \to \pi^0\pi^0$	69.8 ± 21.1
$J/\psi \to \phi f_1$, $f_1 \to \pi^0 f_0, f_0 \to \pi^+\pi^-$	78.2 ± 19.3
$J/\psi \to \phi f_1$, $f_1 \to \pi^0 f_0$, $f_0 \to \pi^0\pi^0$	8.7 ± 6.8 < 18.2 (90% C.L.)
$J/\psi \to \phi\eta'$, $\eta' \to \pi^+\pi^-\pi^0$	183.3 ± 21.0
$J/\psi \to \phi\eta'$, $\eta' \to \pi^0\pi^0\pi^0$	77.6 ± 9.6

the MC simulation for each decay, respectively. B_{YZ}^X is the branching fraction of the decay $X \to YZ$. $N_{J/\psi}$ is the number of J/ψ events. The upper limit of $\mathcal{B}(J/\psi \to \phi f_1, f_1 \to \pi^0 f_0, f_0 \to \pi^0\pi^0)$ is determined according to Eq. (3), where $N_{\mathrm{upp}}^{\mathrm{obs}}$ is the signal yield at the 90% C. L. and σ^{sys} is the total systematic uncertainty, which is described in the next section. Equation (4) is used to calculate the ratio between the branching fraction for $\eta' \to \pi^0\pi^0\pi^0$ and that for $\eta' \to \pi^+\pi^-\pi^0$.

$$\mathcal{B}(J/\psi \to \phi X) = \frac{N^{\mathrm{obs}}}{N_{J/\psi}\epsilon B_{K^+K^-}^\phi (B_{\gamma\gamma}^{\pi^0})^n} \quad (1)$$

$$\mathcal{B}(\eta' \to X) = \frac{N^{\mathrm{obs}}}{N_{J/\psi}\epsilon B_{\phi\eta'}^{J/\psi} B_{K^+K^-}^\phi (B_{\gamma\gamma}^{\pi^0})^n} \quad (2)$$

$$\mathcal{B}(J/\psi \to \phi X) < \frac{N_{\mathrm{upp}}^{\mathrm{obs}}}{N_{J/\psi}\epsilon B_{K^+K^-}^\phi (B_{\gamma\gamma}^{\pi^0})^n (1 - \sigma^{\mathrm{sys}})} \quad (3)$$

$$r_{3\pi} \equiv \mathcal{B}(\eta' \to \pi^0\pi^0\pi^0)/\mathcal{B}(\eta' \to \pi^+\pi^-\pi^0)$$
$$= \frac{N^{\mathrm{obs}}(\pi^0\pi^0\pi^0)}{N^{\mathrm{obs}}(\pi^+\pi^-\pi^0)} \frac{\epsilon(\pi^+\pi^-\pi^0)}{\epsilon(\pi^0\pi^0\pi^0)} \frac{1}{(B_{\gamma\gamma}^{\pi^0})^2} \quad (4)$$

VIII. ESTIMATION OF THE SYSTEMATIC UNCERTAINTIES

(1) *MDC tracking*: The tracking efficiency of kaon tracks is studied using a high purity sample of $J/\psi \to K_S K\pi$ events. The tracking efficiency of the low-momentum pion tracks is studied using a sample of $J/\psi \to \pi^+\pi^- p\bar{p}$ while that of the high-momentum pion tracks is studied using a high statistics sample of $J/\psi \to \rho\pi$. The MC samples and data agree within 1% for each kaon or pion track.

(2) *Photon detection*: The photon detection efficiency is studied using a sample of $J/\psi \to \rho\pi$ events. The systematic uncertainty for each photon is 1% [22].

(3) *PID efficiency*: To study the PID efficiency for kaon tracks, we select a clean sample of $J/\psi \to \phi\eta \to K^+K^-\gamma\gamma$. The PID efficiency is the ratio of the number of events with and without the PID requirement for both kaon tracks. MC simulation is found to agree with data within 0.5%.

(4) *Kinematic fit*: The performance of the kinematic fit is studied using a sample $J/\psi \to \phi\eta \to K^+K^-\pi^+\pi^-\pi^0/K^+K^-\pi^0\pi^0\pi^0$, which has the same final states as the signal channel $J/\psi \to \phi\pi^0 f_0$ with $\phi \to K^+K^-$ and $f_0 \to \pi^+\pi^-/\pi^0\pi^0$. The control sample is selected without using the kinematic constraints. We then apply the same kinematic constraints and the same requirement on the χ^2 from the kinematic fit. The efficiency is the ratio of the yields with and without the kinematic fit. It contributes a systematic uncertainty of 1.0% for $f_0 \to \pi^+\pi^-$ and 2.0% for $f_0 \to \pi^0\pi^0$.

(5) *Veto neutral K^**: In selecting the candidate events $J/\psi \to \phi\pi^0 f_0 \to K^+K^-\pi^+\pi^-\pi^0$, the events with $|M(K^\pm\pi^\mp) - M(K^{*0})| < 0.050$ GeV/c^2 are vetoed to suppress the background containing K^{*0} or $\bar{K}^{*0}$ intermediate states. The requirement is investigated using a clean sample $J/\psi \to \phi\eta \to K^+K^-\pi^+\pi^-\pi^0$. The efficiency is given by the yield ratio with and without the requirement $|M(K^\pm\pi^\mp) - M(K^{*0})| < 0.050$ GeV/c^2. The efficiency difference between data and MC is 0.1%.

(6) *ϕ signal region*: The uncertainty due to the restriction on the ϕ signal region is studied with a high purity sample of $J/\psi \to \phi\eta' \to K^+K^-\pi^+\pi^-\eta$ events as this sample is free of the background $J/\psi \to K^+K^-\eta'$ without the intermediate state ϕ.

(7) *Veto peaking background*: The uncertainties due to the restrictions used to remove peaking background in the mode $\eta' \to 3\pi$ are studied with a control sample of $J/\psi \to \omega\eta \to 2(\pi^+\pi^-\pi^0)$ events. For each sample, the efficiency is estimated by comparing the yields with and without the corresponding requirement. The difference in efficiency between the data and MC samples is taken as the systematic uncertainty.

(8) *Background shape*: To study the effect of the background shape, the fits are repeated with a different fit range or polynomial order. The largest difference in signal yield is taken as the systematic uncertainty.

(9) *Mass resolution*: The mass resolutions, σ_{MC}, from an MC simulation of the modes $f_0 \to \pi^+\pi^-/\pi^0\pi^0$ and $f_1 \to \pi^0 f_0$ have an associated systematic uncertainty. The difference in mass resolution, σ_G, between the data and the MC simulation is determined using a sample of $J/\psi \to \phi\eta$ events where $\eta \to \pi^+\pi^-\pi^0/\pi^0\pi^0\pi^0$. The fit is repeated using different mass resolutions, which are defined as $\sqrt{\sigma_{MC}^2 + \sigma_G^2}$ assuming σ_G is the same for the two-pion and three-pion mass spectra. The difference in yield is taken as a systematic uncertainty.

(10) *MC simulation*: For the decay $J/\psi \to \phi\pi^0 f_0$, the dominant systematic uncertainty is from the efficiency ϵ_0 determined by a phase space MC simulation. The $\pi^0 f_0$ invariant mass spectrum is divided into 5 bins, each with a bin width of 0.2 GeV/c^2. The f_0 signal yields, N_i, are determined by fits to the $\pi\pi$ spectra for each bin i using the mass and width of the f_0 obtained above. The corrected efficiency is $\epsilon_M \equiv \frac{\sum_i N_i}{\sum_i N_i/\epsilon_i}$, where ϵ_i is the efficiency in the i-th bin. The same procedure is applied to the angular distribution of the $\pi^0 f_0$ system in the c.m. frame of the J/ψ to obtain another corrected efficiency ϵ_θ. The difference $\sqrt{(\epsilon_M - \epsilon_0)^2 + (\epsilon_\theta - \epsilon_0)^2}$ is taken as the systematic uncertainty due to the imperfection of the MC simulation.

(11) *f_0 signal region*: For the decay $J/\psi \to \phi f_1$ with $f_1 \to \pi^0 f_0$, the f_0 signal region is $0.960 < M(\pi\pi) < 1.020$ GeV/c^2. The branching fraction measurements are repeated after varying this region to $0.970 < M(\pi\pi) < 1.010$ GeV/c^2 and $0.950 < M(\pi\pi) < 1.030$ GeV/c^2. The differences from the nominal results are taken as the systematic uncertainties due to the signal region of the f_0. For the decay $f_1 \to \pi^0\pi^0\pi^0$, the number of the peaking background $f_1 \to \pi^0\pi^0\eta[\gamma\gamma]$ is determined to be 3.1 ± 0.6. Varying the number of the peaking background within ± 0.6 in the fit, the largest difference of the signal yield gives a systematic uncertainty. The systematic uncertainty values related to the f_1 are shown in brackets in Table II.

(12) *About $\mathcal{B}(J/\psi \to \phi f_1, f_1 \to \pi^0 f_0, f_0 \to \pi^0\pi^0)$*: For the decay $J/\psi \to \phi f_1, f_1 \to \pi^0 f_0$ with $f_0 \to \pi^0\pi^0$, the signal yield at the 90% C. L., $N_{\text{upp}}^{\text{obs}}$ in Eq. (3), is the largest one among the cases with varying the fit ranges, the order of the polynomial describing the background, the number of the peaking background, and the signal region of the f_0 resonance. The total systematic uncertainty, σ^{sys} in Eq. (3), is the quadratic sum of the rest systematic uncertainties in the third column of Table II (the values in the brackets). We obtain $N_{\text{upp}}^{\text{obs}} = 29.0$ and $\sigma^{sys} = 6.9\%$ with the efficiency $(7.21 \pm 0.08)\%$, determined from an MC simulation. $\mathcal{B}(J/\psi \to \phi f_1, f_1 \to \pi^0 f_0, f_0 \to \pi^0\pi^0)$ is calculated to be less than 6.98×10^{-7} at the 90% C. L. according to Eq. (3).

(13) *Uncertainty of $\mathcal{B}(J/\psi \to \phi\eta')$*: For the decay $\eta' \to 3\pi$, the dominant systematic uncertainty arises from the uncertainty of $\mathcal{B}(J/\psi \to \phi\eta') =$

$(4.0 \pm 0.7) \times 10^{-4}$ [1]. A variation in $\mathcal{B}(J/\psi \to \phi\eta')$ will change the size of peaking background and thus the signal yield. In Eq. (2), it is reasonable to consider a change in the quantity $N^{\mathrm{obs}}/B^{J/\psi}_{\phi\eta'}$ with any variation in $\mathcal{B}(J/\psi \to \phi\eta')$. The fit to the data is repeated after varying the number of peaking background to correspond with 1σ variations in $\mathcal{B}(J/\psi \to \phi\eta')$ [1]. The largest difference of $N^{\mathrm{obs}}/B^{J/\psi}_{\phi\eta'}$ from the nominal result is taken as the systematic uncertainty.

(14) *Systematic uncertainties for* $r_{3\pi}$: In the measurement of the ratio $r_{3\pi}$ of $\mathcal{B}(\eta' \to \pi^0\pi^0\pi^0)$ over $\mathcal{B}(\eta' \to \pi^+\pi^-\pi^0)$, the systematic uncertainties due to the reconstruction and identification of kaon tracks and photon detection cancel as the efficiency ratio $\epsilon(\pi^0\pi^0\pi^0)/\epsilon(\pi^+\pi^-\pi^0)$ appears in Eq. (4). The effect of the uncertainty in the number of peaking background due to the uncertainty of $\mathcal{B}(J/\psi \to \phi\eta')$ is also considered.

All systematic uncertainties including those on the number of J/ψ events [12] and other relevant branching fractions from the PDG [1] are summarized in Table II, where the total systematic uncertainty is the quadratic sum of the individual contributions, assuming they are independent. Efficiency and branching fraction measurements are summarized in Table III.

IX. SUMMARY

In summary, we have studied the decay $J/\psi \to \phi 3\pi \to K^+K^-3\pi$. The isospin violating decay $J/\psi \to \phi\pi^0 f_0$ is observed for the first time. In the $\pi^0 f_0$ mass spectrum, there is an evidence of the axial-vector meson f_1, but not all $\pi^0 f_0$ pairs come from the decay of an f_1. Using $\mathcal{B}(J/\psi \to \phi f_1) = (2.6 \pm 0.5) \times 10^{-4}$ and $\mathcal{B}(f_1 \to \pi a_0 \to \pi\pi\eta) = (36 \pm 7)\%$ from the PDG [1], the ratio $\mathcal{B}(f_1 \to \pi^0 f_0 \to \pi^0\pi^+\pi^-)/\mathcal{B}(f_1 \to \pi^0 a_0^0 \to \pi^0\pi^0\eta)$ is determined to be $(3.6 \pm 1.4)\%$ assuming isospin symmetry in the decay $f_1 \to a_0\pi$. This value is only about $1/5$ of $\mathcal{B}(\eta(1405) \to \pi^0 f_0 \to \pi^0\pi^+\pi^-)/\mathcal{B}(\eta(1405) \to \pi^0 a_0^0 \to \pi^0\pi^0\eta) = (17.9 \pm 4.2)\%$ [4]. On the other hand, the measured mass and width of the f_0 obtained from the invariant dipion mass spectrum are consistent with those in the decay $J/\psi \to \gamma\eta(1405) \to \gamma\pi^0 f_0$ [4]. The measured f_0 width is much narrower than the world average value of $40-100$ MeV [1]. It seems that there is a contradiction in the isospin-violating decays $f_1/\eta(1405) \to \pi^0 f_0$. However, a recent theoretical work [23], based on the triangle singularity mechanism as proposed in Ref. [5, 6], analyzes the decay $f_1 \to \pi^0 f_0 \to \pi^0\pi^+\pi^-$ and predicts that the width of the peaking structure in the f_0 region is about 10 MeV. It also derives $\mathcal{B}(f_1 \to \pi^0 f_0 \to \pi^0\pi^+\pi^-)/\mathcal{B}(f_1 \to \pi^0 a_0^0 \to \pi^0\pi^0\eta) \simeq 1\%$, which is close to our measurement. This analysis supports the argument that the nature of the resonances a_0^0 and f_0 as dynamically generated

makes the amount of isospin breaking strongly dependent on the physical process [23]. In addition, we have measured the branching fractions $\mathcal{B}(\eta' \to \pi^+\pi^-\pi^0) = (4.28 \pm 0.49(\mathrm{stat.}) \pm 0.22(\mathrm{syst.}) \pm 1.09) \times 10^{-3}$ and $\mathcal{B}(\eta' \to \pi^0\pi^0\pi^0) = (4.79 \pm 0.59(\mathrm{stat.}) \pm 0.33(\mathrm{syst.}) \pm 1.09) \times 10^{-3}$, where the last uncertainty is due to $\mathcal{B}(J/\psi \to \phi\eta')$. The ratio between them $r_{3\pi} = 1.12 \pm 0.19(\mathrm{stat.}) \pm 0.06(\mathrm{syst.})$ is also measured for the first time. These results are consistent with those measured in the decay $J/\psi \to \gamma\eta'$ [4].

TABLE II. Summary of systematic uncertainties (%). For $f_0 \to \pi\pi$, the values in the brackets are for the decay $f_1 \to \pi^0 f_0$. For $\eta' \to 3\pi$, the systematic uncertainty from the uncertainty of $\mathcal{B}(J/\psi \to \phi\eta')$ is not included in the total quadratic sum. The last column lists the systematic uncertainties for the ratio between $\mathcal{B}(\eta' \to \pi^0\pi^0\pi^0)$ and $\mathcal{B}(\eta' \to \pi^+\pi^-\pi^0)$, denoted by $r_{3\pi}$.

Sources	$f_0 \to \pi^+\pi^-$	$f_0 \to \pi^0\pi^0$	$\eta' \to \pi^+\pi^-\pi^0$	$\eta' \to 3\pi^0$	$r_{3\pi}$
MDC tracking	4.0	2.0	4.0	2.0	2.0
Photon detection	2.0	6.0	2.0	6.0	4.0
PID efficiency	0.5	0.5	0.5	0.5	-
Kinematic fit	1.0	2.0	1.0	2.0	1.5
Veto neutral K^*	0.1	-	-	-	-
ϕ signal region	1.1	1.1	1.1	0.5	0.5
Veto peaking bkg.	-	-	0.3	0.9	0.9
Bkg. shape	5.4 (15.5)	4.4 (15.6)	1.3	0.3	1.4
Mass resolution	0.3 (0.4)	1.0 (0.1)	-	-	-
MC simulation	11.4 (-)	11.4 (-)	-	-	-
f_0 signal region	-(2.4)	-(68.2)	-	-	-
$\mathcal{B}(J/\psi \to \phi\eta')$	-	-	25.6	22.8	-
Peaking bkg.	-	-(6.9)	-	-	2.2
Number of J/ψ	0.8	0.8	0.8	0.8	-
Other B.F.	1.0	1.0	1.0	1.0	0.1
Total	13.6 (16.5)	14.5 (70.6)	5.1	6.9	5.5

TABLE III. Summary of the efficiencies and the branching fractions. For the branching fractions, the first error indicates the statistical error and the second the systematic error. For $\mathcal{B}(\eta' \to 3\pi)$, the third error is due to the uncertainty of $\mathcal{B}(J/\psi \to \phi\eta')$ [1]. The last line gives the measured value of $r_{3\pi}$, defined as $\mathcal{B}(\eta' \to \pi^0\pi^0\pi^0)/\mathcal{B}(\eta' \to \pi^+\pi^-\pi^0)$.

Decay mode	Efficiency (%)	Branching fractions
$J/\psi \to \phi\pi^0 f_0, f_0 \to \pi^+\pi^-$	12.44 ± 0.10	$(4.50 \pm 0.80 \pm 0.61) \times 10^{-6}$
$J/\psi \to \phi\pi^0 f_0, f_0 \to \pi^0\pi^0$	6.76 ± 0.08	$(1.67 \pm 0.50 \pm 0.24) \times 10^{-6}$
$J/\psi \to \phi f_1, f_1 \to \pi^0 f_0 \to \pi^0\pi^+\pi^-$	13.19 ± 0.11	$(9.36 \pm 2.31 \pm 1.54) \times 10^{-7}$
$J/\psi \to \phi f_1, f_1 \to \pi^0 f_0 \to \pi^0\pi^0\pi^0$	6.76 ± 0.08	$(2.08 \pm 1.63 \pm 1.47) \times 10^{-7}$
		$< 6.98 \times 10^{-7}$ (90% C. L.)
$\eta' \to \pi^+\pi^-\pi^0$	16.92 ± 0.12	$(4.28 \pm 0.49 \pm 0.22 \pm 1.09) \times 10^{-3}$
$\eta' \to \pi^0\pi^0\pi^0$	6.55 ± 0.08	$(4.79 \pm 0.59 \pm 0.33 \pm 1.09) \times 10^{-3}$
$r_{3\pi}$		$1.12 \pm 0.19 \pm 0.06$

[1] K. A. Olive *et al.* (Particle Data Group), Chin. Phys. C **38**, 090001 (2014).

[2] N. N. Achasov, S. A. Devyanin, G. N. Shestakov, Phys. Lett. B **88**, 367 (1979).

[3] M. Ablikim *et al.* (BESIII Collaboration), Phys. Rev. D **83**, 032003 (2011).

[4] M. Ablikim *et al.* (BESIII Collaboration), Phys. Rev. Lett. **108**, 182001 (2012).

[5] J. J. Wu, X. H. Liu, Q. Zhao, B. S. Zou, Phys. Rev. Lett. **108**, 081803 (2012).

[6] F. Aceti, W. H. Liang, E. Oset, J. J. Wu, and B. S. Zou, Phys. Rev. D **86**, 114007 (2012).

[7] F. Binon *et al.* (IHEP-IISN-LAPP Collaboration), Phys. Lett. B **140**, 264 (1984).

[8] D. Alde *et al.* (IHEP-IISN-LANL-LAPP Collaboration), Z. Phys. C **36**, 603 (1987).

[9] A. Blik *et al.*, Phys. Atom. Nucl. **71**, 2124 (2008).

[10] D. J. Gross, S. B. Treiman, F. Wilczek, Phys. Rev. D **19**, 2188 (1979).

[11] M. Ablikim *et al.* (BESIII Collaboration), Chin. Phys. C **36**, 915 (2012).

[12] The total number of J/ψ events taken in 2009 and 2012 is determined to be 1.311×10^9 with an uncertainty 0.8% with the same approach in Ref. [11].

[13] M. Ablikim *et al.*, Nucl. Instrum. Meth. Phys. Res. A **614**, 345 (2010).

[14] G. Barrand *et al.*, Comput. Phys. Commun. **140**, 45 (2001).

[15] S. Agostinelli *et al.*, (GEANT4 Collaboration), Nucl. Instrum. Meth. A **506**, 250 (2003).

[16] D. J. Lange, Nucl. Instrum. Meth. A **462**, 152 (2001).

[17] R. G. Ping, Chin. Phys. C **32**, 599 (2008).

[18] J. C. Chen, G. S. Huang, X. R. Qi, D. H. Zhang, Y. S. Zhu, Phys. Rev. D **62**, 034003(2000).

[19] M. Ablikim *et al.* (BES Collaboration), Phys. Lett. B **607**, 243 (2005).

[20] F. James *et al.*, Statistic Methods in Experimental Physics (2nd edition, World Scientific, 2007).

[21] M. Ablikim *et al.* (BESIII Collaboration), Phys. Rev. D **91**, 052017 (2015).

[22] M. Ablikim *et al.* (BESIII Collaboration), Phys. Rev. D **83**, 112005 (2011).

[23] F. Aceti, J. M. Dias and E. Oset, Eur. Phys. J. A **51**, 48 (2015)